ACS Catalysis

pubs.acs.org/acscatalysis Research Article

# Simultaneously Achieving High Conversion and Selectivity in Syngas-to-Propane Reaction via a Dual-Bed Catalyst System

Zhaopeng Liu, Youming Ni, Mingbin Gao, Linying Wang, Xudong Fang, Jie Liu, Zhiyang Chen, Nan Wang, Peng Tian, Wenliang Zhu,* and Zhongmin Liu*

Cite This: *ACS Catal.* 2022, 12, 3985−3994 Read Online

ACCESS | Metrics & More | Article Recommendations | Supporting Information

**ABSTRACT:** Given the increase in global carbon emissions, efficiently converting syngas into one single $C_{2+}$ hydrocarbon product with low $CO_2$ selectivity is important but still challenging. Herein, we report a dual-bed catalyst system, which can highly convert syngas into propane with lower $CO_2$ emissions. Propane in hydrocarbon products can reach 79% at CO conversion of 96% with 12% $CO_2$ selectivity. The selectivity of methane is lower than 6% at the same time. Furthermore, up to 66% propane yield is achieved, which can significantly increase the efficiency of carbon utilization compared with traditional methods. The catalytic performance of the dual-bed reaction system also exhibits an excellent stability during the 200 h test on stream. The dual-bed reaction system is configured with a syngas-to-dimethyl ether (DME) $CuZnAlO_x$ + ZSM-5 catalyst in the upper bed and a DME-to-propane SSZ-13 zeolite catalyst in the lower bed. The higher strength of the acid sites for SSZ-13 benefits the formation of propane and helps to limit the coke deposition. Probing experiments and DFT calculations imply that syngas-to-propane reaction includes methanol-to-olefin processes and subsequent conversion of lower olefins in high-pressure $H_2$. The generated intermediate propylene hydrogenation over SSZ-13 leads to a high propane selectivity. This strategy offers a scenario to promote the syngas-to-hydrocarbon performance with low $CO_2$ emissions.

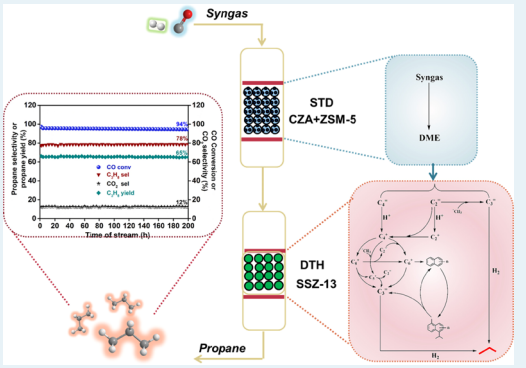


**KEYWORDS:** *syngas-to-propane, dual-bed, $CuZnAlO_x$ + ZSM-5, SSZ-13*

## 1. INTRODUCTION

With the depletion of petroleum resources and the arrival of carbon neutrality, the development of a nonpetroleum route for producing fuels and bulk chemicals is of great significance. Among various alternative routes, syngas conversion is very attractive because the technologies for syngas production from many nonpetroleum resources like biomass and $CO_2$ are industrially applied. Until now, a variety of hydrocarbon fuels (i.e., gasoline and diesel) and chemicals (i.e., light olefins and aromatics) have been synthesized from syngas by using Fischer−Tropsch (F−T)[1−6] or oxide−zeolite (OX-ZEO) bifunctional catalysts.[7−11] Due to the control of Anderson−Schulz−Flory distribution, it is not easy to obtain a single hydrocarbon product by conventional F−T synthesis. Recently, with the progress of OX-ZEO catalyst design, some single hydrocarbons, such as ethane,[12] ethylene,[13] propane,[14,15] and tetra-methylbenzene,[16] have been synthesized with a relatively higher selectivity, but the yield of the target product is still unsatisfactory. In our opinion, there are at least two reasons for the low yield. The oxide components such as $ZnCrO_x$ and $ZnZrO_x$ in OX-ZEO catalysts are not highly effective for converting syngas. Moreover, the selectivity of $CO_2$ is too high and generally reaches 40−50%.

During the OX-ZEO catalysis process, the intermediate oxygenated compounds (such as methanol and dimethyl ether) generated on oxides are transformed into hydrocarbons and water on zeolites. The water continues to react with CO to form $CO_2$ on oxides by water-gas-shift (WGS) reaction. Since the zeolite and oxide components are completely bonded together, the severe WGS reaction is difficult to avoid. In order to solve all above problems, we proposed the design concept of a dual-bed reaction system. High efficiency syngas-to-dimethyl ether (so-called STD) catalysts, such as $CuZnAlO_x$ + ZSM-5 and $CuZnAlO_x$ + $\gamma$-$Al_2O_3$, were placed on the upper bed, while DME-to-hydrocarbon catalysts such as SAPO-34 and H-ZSM-5 were put on the lower bed. By using the dual-bed reaction system, syngas was highly converted to lower olefins ($C_2$−$C_4^=$) or gasoline ranged hydrocarbons.[17−19] However, so far,

Received: November 8, 2021
Revised: March 3, 2022







https://doi.org/10.1021/acscatal.1c05132
*ACS Catal.* 2022, 12, 3985−3994

obtaining a highly selective one hydrocarbon product with high CO conversion is still challenging in syngas conversion.

Herein, we report a dual-bed catalyst system containing a syngas-to-dimethyl ether (DME) catalyst $CuZnAlO_x$ + ZSM-5 in the upper bed and a DME-to-hydrocarbon zeolite catalyst SSZ-13 in the lower bed. The reaction temperatures of the dual-bed catalyst can be separately controlled (Scheme 1). The propane in the hydrocarbon product can reach 79% at CO conversion of 96% with 12% $CO_2$ selectivity. The propane yield is up to 66%. As expected, this dual-bed configuration mode can realize that each catalyst operates at its optimistic reaction temperature, which exhibits superior performance in syngas-to-propane reaction. The propane formation mechanism is also explored.

**Scheme 1. Configuration of the Dual-Bed Catalyst System for Syngas-to-Propane Reaction**

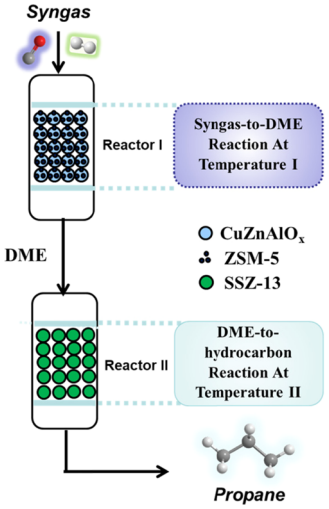


## 2. EXPERIMENTAL SECTION

**2.1. Catalyst Preparation.** The methanol synthesis catalysts of $ZnCrAlO_x$ and $CuZnAlO_x$ were prepared by a traditional coprecipitation method.[7,20] The molar ratio of Cu/Zn/Al for the $CuZnAlO_x$ catalyst was about 6:3:1, while that of Zn/Cr/Al for the $ZnCrAlO_x$ catalyst was about 1:1:2. SAPO-18, SAPO-34, ZSM-5, and SSZ-13 ($SiO_2/Al_2O_3$ ratio = 12 and 20) zeolites were all commercially supplied. SSZ-13 zeolites ($SiO_2/Al_2O_3$ ratio = 34 and 60) were supplied by 1202 Group in Dalian Institute of Chemical Physics (DICP). The commercial Na-SSZ-13 ($SiO_2/Al_2O_3$ = 12.5) was converted into H-form by exchanging Na-SSZ-13 with $NH_4NO_3$ aqueous solution (a series of concentrations of 0.01, 0.03, 0.1, 0.3, and 1 $mol^{-1}$ $L^{-1}$) at 353 K for 2 h followed by filtration and washing with deionized water. The desired samples were dried at 383 K for 10 h followed by calcination at 823 K for another 4 h in air to obtain a series of SSZ-13-*x*%$H^+$ zeolites (where "*x*" indicates $H^+$-exchange, which was determined by 100-(Na/Al)mol %; SSZ-13-100%$H^+$ was denoted as SSZ-13 in this work).

The hybrid catalysts OX + ZEO (such as $ZnCrAlO_x$ + SSZ-13, $CuZnAlO_x$ + SSZ-13, and $CuZnAlO_x$ + ZSM-5) were obtained by mechanically mixing granules (0.4−0.8 mm) of two components. The weight ratio of oxide and zeolite for the hybrid catalyst was 2:1.

Catalysts in the dual-bed reaction system (such as $CuZnAlO_x$/SSZ-13 and ($CuZnAlO_x$ + ZSM-5)/SSZ-13) used in this work were composed of syngas-to-methanol catalyst $CuZnAlO_x$ oxide or the syngas-to-DME catalyst $CuZnAlO_x$ + ZSM-5 in the upper bed and SSZ-13 zeolite in the lower bed. The weight ratio of upper bed catalyst and lower bed catalyst was 3:1.

**2.2. Catalyst Characterizations.** The X-ray diffraction patterns were tested with a PANalytical X'Pert PRO X-ray diffractometer with Cu K$\alpha$ radiation. Elemental analysis was carried out using a Philips Magix-601 X-ray fluorescence spectrometer. The BET surface areas, average pore width, and pore volumes of all the samples were estimated by nitrogen adsorption−desorption isotherms at 77 K using a Micromeritics ASAP 2020 apparatus. Temperature programmed desorption of ammonia ($NH_3$-TPD) analysis was performed using 100 mg of powder of the zeolite at a temperature range of 350−1000 K after the sample pretreatment at 723 K for 1 h under a He flow using a Micromeritics Autochem II 2920 equipped with a thermal conductivity detector (TCD).

In situ diffuse reflection infrared Fourier transform spectroscopy (DRIFTS) studies were carried out with a Bruker Tensor 27 instrument with an MCT detector to detect the change of intensity of surface intermediate species. Then, 50 mg of sample powder was pressed into a diffuse reflectance infrared cell with a ZnSe window. Prior to the in situ DRIFTS test, the catalyst was treated under $N_2$ flow at 673 K for 4 h, and then, the catalyst was cooled down to 653 K. The background spectrum was obtained at 653 K. Then, the catalyst sample was exposed to an $H_2$/DME mixture (2 mL/min DME and 30 mL/min $H_2$), and the catalyst was treated at this temperature for 30 min. After this, the temperature was ramped every 10 K from 653 to 703 K, and the temperature was kept for about 20 min for recording. The FT-IR spectra of the surface species generated on the catalyst were obtained. In situ DRIFTS spectra were recorded with a Nicolet FTIR spectrometer with a resolution of 2 $cm^{-1}$ and scan numbers of 32.

**2.3. Catalytic Performance Test.** Syngas conversion was performed on a dual-bed reaction system (shown in Scheme 1 in the Section 1), which contained two fixed-bed stainless reactors in tandem (one upper reactor linked with another). Each bed was equipped with a temperature controller, and the reaction temperatures of these two beds could be controlled independently. The syngas-to-propane reaction occurred at 533 K (upper bed catalyst) and 683 K (lower bed catalyst), 5.0 MPa. For comparison, the catalytic behavior of syngas conversion was also performed over the OX + ZEO hybrid catalyst (such as $ZnCrAlO_x$ + SSZ-13 and $CuZnAlO_x$ + SSZ-13 at 683 K, 5.0 MPa). All products were kept in the gas phase and analyzed online with an Agilent 7890B GC equipped with an HP-PLOT/Q capillary column connected to an FID detector and a TDX-1 column connected to a TCD detector. $CH_4$ was used as a reference bridge between TCD and FID. Hydrocarbon selectivity was based on the carbon atom number. CO conversion, hydrocarbons ($C_nH_m$), MeOH, and DME selectivity calculation methods (excluding $CO_2$) were the same as our previous work.[21]

**2.4. Thermogravimetric Analysis of Zeolite after Reaction and Confined Organic Determination with UV−Vis and GC−MS.** Thermogravimetric analysis (TGA) was performed with a TA Q-600 analyzer with a heating rate of 10 K/min from room temperature to 1200 K under the air flow. UV−vis spectra were recorded on a Cary 5000 spectrophotometer. The used zeolites loaded in the lower


https://doi.org/10.1021/acscatal.1c05132
ACS Catal. 2022, 12, 3985−3994

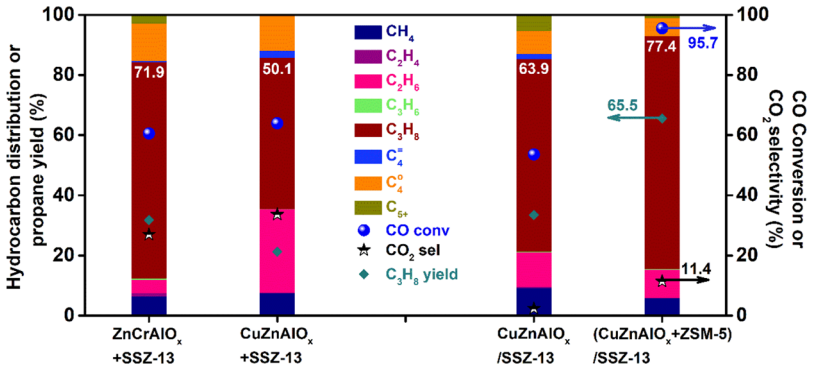


**Figure 1.** Catalytic performance of syngas conversion over various catalysts. (OX + ZEO) is the hybrid mode catalyst, prepared by granule mixing of 0.6 g of oxide with 0.3 g of zeolite, $P$ = 5.0 MPa, $T$ = 683 K, $H_2/CO$ = 7, and GHSV = 4000 mL $g^{-1}$ $h^{-1}$. Catalyst A/Catalyst B represents catalysts in the dual-bed reaction system, configured by 0.6 g of catalyst A in the upper bed and 0.2 g of catalyst B in the lower bed, $T$ (upper bed) = 533 K, $T$ (lower bed) =683 K, $P$ = 5.0 MPa, $H_2/CO$ = 7, and GHSV = 4000 mL $g^{-1}$ $h^{-1}$.

bed were pressed into the diffuse reflectance cell. Before the UV−vis test, the catalyst was treated at 673 K for 2 h with 20 mL/min $N_2$ flow. The UV−vis spectra of the used samples (100 mg) were recorded in air against $BaSO_4$ in the region of 200−800 nm and scanning speed at 600 nm/min. The organic materials retained in the spent zeolites after reactions were analyzed by M. Guisnet's method.[22] The spent zeolites were dissolved in 20 wt % HF solution. After being neutralized with 5 wt % sodium hydroxide solution, the soluble organics were extracted with $CH_2Cl_2$ (containing 10 ppm $C_2Cl_6$ as an inner standard) and then analyzed with a GC−MS instrument (Agilent 7890B) equipped with an HP-5 capillary column.

**2.5. Density Functional Theory (DFT) Calculations.** DFT calculations were performed with the Gaussian 09 package. For the calculation of the transition state, an extended 74 T ($Si73AlO119H59$) cluster model extracted from the crystallographic CHA structure represents the structure of the neutral H-SSZ-13 model containing one Brønsted acid site as shown in Figure S3. For the extended model, the terminal Si−H was fixed and oriented along the direction of the corresponding Si−O bond. The location of the acid site was chosen at the 8-membered ring, which is accessible for adsorbents and surrounded by the maximum reaction space. To preserve the integrity of the crystalline structure, the 8-membered ring, active center $(SiO)_3$−Si−OH−Al−$(SiO)_3$ and the adsorbate were set to a high-level layer, while the rest of the atoms were set to a low-level layer. The combined theoretical ONIOM method was exploited to predict the stability of various adsorption structures, geometries, and transition states (TS). For the structure optimization, ωB97XD hybrid density functions with 6-31G(d,p) basis sets and semi-empirical AM1 were employed for optimization of the structures of high-level and low-level layers, respectively. To obtain a highly accurate interaction energy, the single-point energies were calculated at the level of ωB97XD/6-31G(d,p) on the basis of the optimized structure. The frequency calculations were performed at the same level as geometry optimizations to check whether the saddle point exhibits the appropriate number of imaginary frequencies. The attained TS is a first-order saddle point of the potential energy surface, with only a single imaginary frequency. The adsorbed state is verified as being situated in the energy minima points of the potential energy surface, with only real frequency. The intrinsic free energy was obtained from the ωB97XD/6-31G(d,p) total electronic energies and the thermal correction from the ωB97XD/6-31G(d,p): AM1 frequency calculations with the correction of zero-point vibration energies. Reactions: (H-OZ represents the zeolite framework with Brønsted acidity).

## 3. RESULTS AND DISCUSSION

**3.1. Physicochemical Properties of Oxides and Zeolites Used in This Work.** The physicochemical properties of the samples used in this work for the syngas-to-propane reaction are shown in Table S1. Figure S1a,b indicates that all the SSZ-13 and SAPO-34 have a typical CHA structure, and SAPO-18 exhibits a typical AEI structure. As shown in Figure S2a,b, the $NH_3$-TPD profiles present two peaks ascribed to weak and strong acid sites,[23] respectively. The results demonstrate that the acid strength for all the SSZ-13 zeolites is much stronger than that of SAPOs (such as SAPO-34 and SAPO-18). In addition, the acid strength increases as the $H^+$-exchanging degree increases but decreases with the ratio of $SiO_2/Al_2O_3$ climbing. Table S2 indicates that the acid amount follows the order SAPO-34 > SAPO-18 > SSZ-13. The acid amount of SSZ-13 zeolite increases with increasing $H^+$-exchange while decreasing with the $SiO_2/Al_2O_3$ ratio climbing.

**3.2. Catalytic Performance of Syngas-to-Propane over Various Catalysts.** We compared the behaviors of syngas-to-propane over different catalysts at 5.0 MPa with identical space velocity (GHSV). As shown in Figure 1 and Table S3, the hybrid catalyst $ZnCrAlO_x$ + SSZ-13 exhibits a 71.9% propane selectivity at 60.6% CO conversion with about 30% $CO_2$ selectivity. The performance of $CuZnAlO_x$ oxide mixed with SSZ-13 is also investigated. As expected, higher CO conversion and $CO_2$ selectivity were obtained. Note that the propane selectivity declined to 50.1% with undesired 27.2% ethane and 13.7% butane in hydrocarbons. This is possibly attributed to strong ability of hydrogenation within the $CuZnAlO_x$ catalyst, which leads to a rapid hydrogenation of $C_2$−$C_4$ olefins in high-pressure $H_2$. Separation of $CuZnAlO_x$ oxide and SSZ-13 zeolite, that is, the dual-bed system with zeolite downstream from oxide, $CuZnAlO_x$/SSZ-13, exhibits a high CO conversion of 54.1% with 63.9% propane selectivity. More interestingly, the generated $CO_2$ amount (3%) is much smaller than that of all above hybrid catalysts. When $CuZnAlO_x$ is physically mixed with H-ZSM-5, ($CuZnAlO_x$ + ZSM-5)/SSZ-13, which is configured by $CuZnAlO_x$ + ZSM-5 in the upper bed and SSZ-13 in the lower bed, exhibits a much better performance than all above catalysts. CO conversion reaches 95.7% with 77.4% propane selectivity, and the


https://doi.org/10.1021/acscatal.1c05132
ACS Catal. 2022, 12, 3985−3994

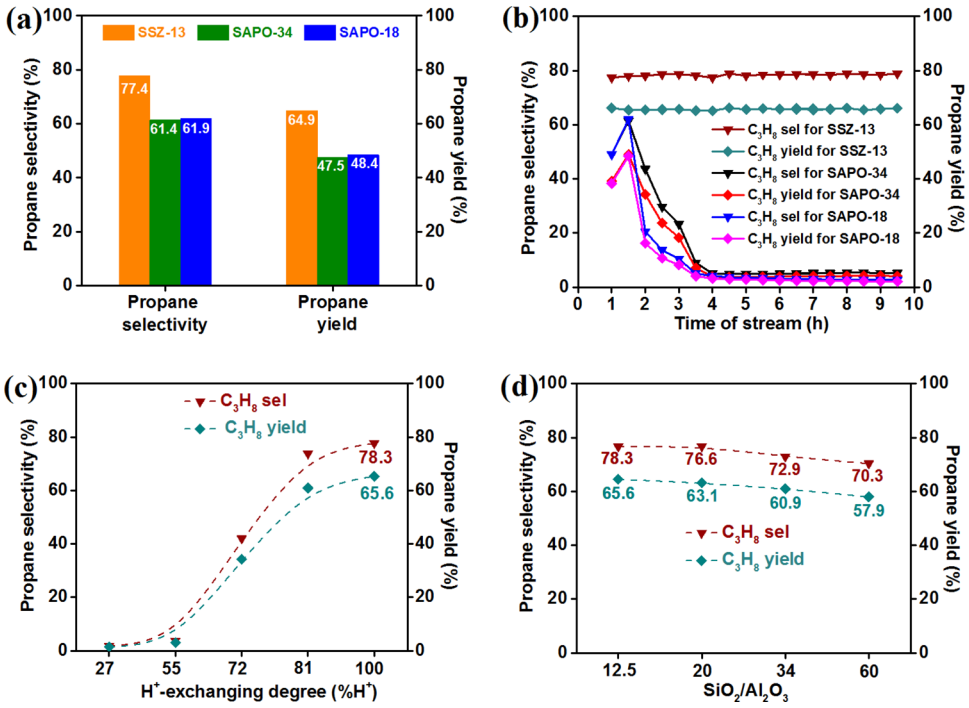


**Figure 2.** Propane selectivity and yield of syngas conversion in the dual-bed reaction system. $T$ (upper bed) = 533 K, $T$ (lower bed) = 683 K, $P$ = 5.0 MPa, $H_2/CO$ = 7, GHSV = 4000 mL $g^{-1}$ $h^{-1}$. (a) Effect of different zeolites in the lower bed on propane selectivity and yield over ($CuZnAlO_x$ + ZSM-5)/zeolite; (b) stability of zeolite in ($CuZnAlO_x$ + ZSM-5)/zeolite for the syngas-to-propane reaction; (c) effect of the $H^+$-exchanging degree of SSZ-13 zeolite in ($CuZnAlO_x$ + ZSM-5)/SSZ-13; and (d) effect of the $SiO_2/Al_2O_3$ ratio of SSZ-13 zeolite in ($CuZnAlO_x$ + ZSM-5)/SSZ-13.

selectivity of undesired $CO_2$ is suppressed to 11.4%. Furthermore, ($CuZnAlO_x$ + ZSM-5)/SSZ-13 presents a propane yield up to 65.5%, which is 2 times as high as that of the $ZnCrAlO_x$ + SSZ-13 hybrid catalyst and $CuZnAlO_x$/SSZ-13. This result is much higher than that reported in the previous literature (Table S4).[14,24−28]

**3.3. The Effect of Reaction Conditions on the CO Conversion.** In the previous work of the dual-bed mode catalyst for syngas-to-olefin reaction (DSTO) process,[17] the STD reaction dominates CO conversion and $CO_2$ selectivity. In order to pursue an efficient syngas conversion process, further enhancing the single-pass conversion of CO and suppressing the selectivity of $CO_2$ are definitely needed. As demonstrated in Figure S4a and S4c, CO conversion in STD reaction could approach the value predicted by the thermodynamic equilibrium under some reaction conditions, which are more effective than the syngas-to-methanol (MeOH) reaction. Figure S4b indicates that more than 90% CO conversion can be achieved only below 563 K. Continuing to raise the reaction temperature is disadvantageous to STD reaction. According to the previous literature,[29] WGS reaction would be severe at high temperatures. Therefore, we choose 533 K for the STD process. Figure S4c shows that CO conversion is increased with the $H_2/CO$ ratio climbing. Figure S4d indicates that increasing space velocity is not beneficial to high CO conversion.

**3.4. The Effect of Zeolites on the Selectivity of Propane.** Our previous studies[17−19] clearly proved that zeolites loaded in the lower bed are responsible for product distribution in syngas conversion and the 8-membered ring microporous zeolites showed high selectivity for low-carbon hydrocarbon species. Therefore, three kinds of small pore molecular sieves (SAPO-18, SAPO-34, and SSZ-13) were investigated. In the case of SAPO-34 (with the same CHA-topology as SSZ-13) and SAPO-18 (with AEI-topology), which are all suitable for highly selective propane (shown in Figure 2a), the propane selectivity in the dual-bed reaction system achieved approximately 61% in the time of stream (TOS) of 1.5 h (Figure 2b). After this, the propane selectivity declined quickly, and DME and MeOH increased. Compared with SAPO-34 or SAPO-18 in the syngas-to-propane process, in the lower bed, SSZ-13 zeolite exhibits an excellent stability under the same reaction conditions (Figure 2b). The effect of acidity of SSZ-13 zeolite in the lower bed is also investigated; Figure 2c,d indicates that increasing the $H^+$-exchanging degree can significantly increase the propane selectivity from 1.8 to 77.6%, while increasing the $SiO_2/Al_2O_3$ ratio (SAR) could slightly decrease the propane selectivity.

**3.5. TGA, UV−vis, and GC−MS Analysis of Organic Species in the Spent Zeolites.** The spent SSZ-13, SAPO-18, and SAPO-34 molecular sieves were analyzed by TGA. As presented in Figure 3a, a low-temperature weight loss at <450 K and a high-temperature weight loss at >600 K can be recognized. The former temperature range can be ascribed to desorption of volatile compounds, while the latter temperature range is assigned to coke compounds.[30] Table S5 summarizes the TG analysis results of all samples used for syngas-to-propane in the lower bed. By calculation, the average formation rates of retained species SAPO-34 and SAPO-18 are all higher than those of SSZ-13 zeolite. This indicates that compared with SAPOs with 8-MR micropores, SSZ-13 zeolite is more resistant to carbon deposition deactivation. In addition, SSZ-13 zeolite with a lower $SiO_2/Al_2O_3$ ratio (with a higher acid strength) is beneficial to inhibiting carbon deposition. The nature of organic species formed in the spent zeolites was also investigated by ex situ UV−vis spectroscopy. Figure 3b


https://doi.org/10.1021/acscatal.1c05132
ACS Catal. 2022, 12, 3985−3994

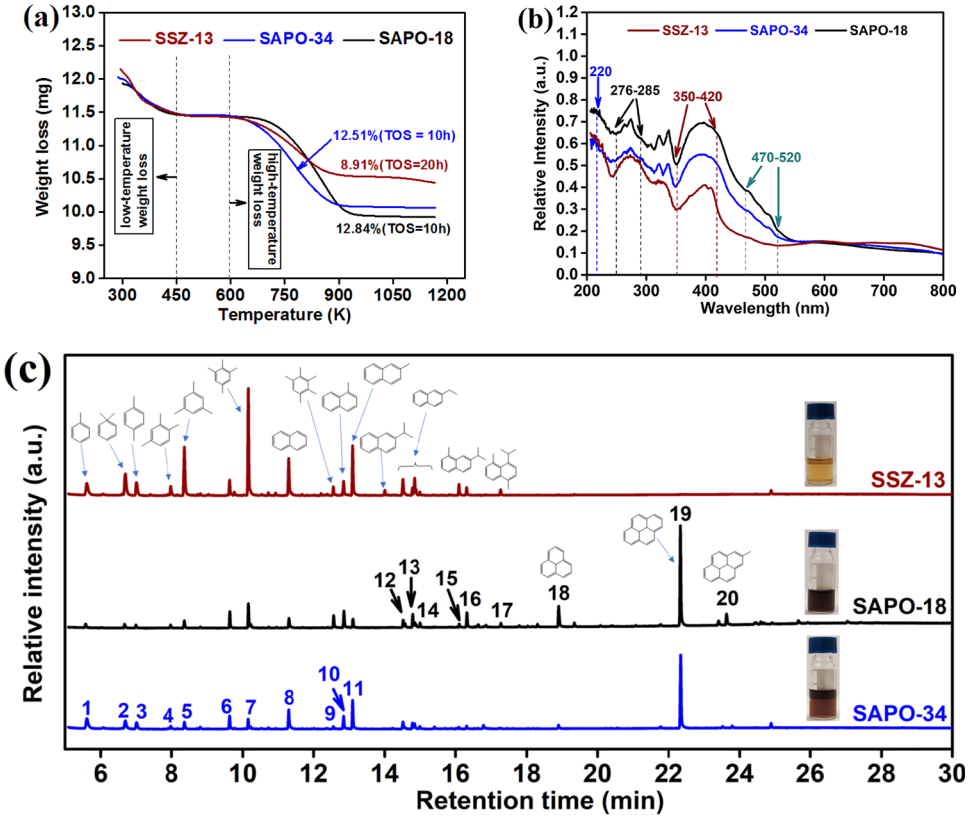


**Figure 3.** (a) TG curves of the spent zeolites; (b) ex situ UV−vis spectra of the spent zeolites obtained after the reaction; (c) GC−MS chromatograms of the organic materials retained in zeolite components of spent ($CuZnAlO_x$ + ZSM-5)/zeolite, $C_2Cl_6$ was used as the internal standard, methyl-benzene, (2 or 3): dimethyl-benzene, (4 or 5): trimethyl-benzene, 6: C2Cl6, 7: tetamethyl-benzene, 8: naphthalene, 9: pentamethyl-benzene, (10 or 11): methyl-naphthalene, 12: dimethyl-naphthalene, 13: trimethyl-naphthalene, (14−17): polymethyl-isopropylnaphthalenes: 18: phenanthrene, 19: pyrene, and 20: methyl-pyrene.

indicates that the UV bands at 220−420 nm occurred in all above samples. The band at 220 nm is attributed to dienes,[30,31] which fits well with the performance of the lower-temperature weight loss in the TG analysis. Broad bands at 276−285 and 350−420 nm are attributed to the methylated benzenes and polycyclic aromatic species,[32,33] respectively, which suggested that carbon chain growth and aromatization processes occurred in syngas-to-propane over all above the mentioned zeolites in the lower bed. Compared with SSZ-13 zeolite, additional bands at 470−520 nm occurred in SAPO-34 and SAPO-18 zeolites, which are attributed to the condensed aromatics with two or three aromatic species with more than three or four rings.[34,35] As is well known, the condensed aromatic species are generally considered as coke deposits that cause deactivation by covering the acid center sites.[36] The concentrations of all above organic species are reflected by the intensities of the corresponding UV bands, which are consistent with the order of weight losses in TG analysis. To further confirm the nature of organic species over spent zeolites, we dissolved the spent SSZ-13, SAPO-34, and SAPO-18 zeolites by using HF and extracted the retained organics by $CH_2Cl_2$, and then analyzed soluble organics by GC−MS. As shown in Figure 3c, compared with the soluble organic solutions of the spent SAPO-34 and SAPO-18 samples, the color of the extract of the spent SSZ-13 zeolite becomes lighter and the detailed analysis of GC−MS results indicates that light aromatics such as methylbenzenes (species 1−7 and 9), naphthalene (species 8), and methylnaphthalenes (species 10−17) can be observed in the spent SSZ-13 zeolite, with no condensed aromatics (such as phenanthrene and pyrene etc.) detected in the residues. However, the content of all the above light aromatic species is much less than that in SAPO-34 and SAPO-18 due to the presence of phenanthrene and pyrene, which are in good agreement with UV−vis results. The accumulation of these polycyclic aromatics would lead to blocking of molecular sieve pores and cause the deactivation of the catalyst.[37] Based on the previous literature,[37,38] aromatics hydrogen could take place over acid sites on zeolites under a high-pressure $H_2$ atmosphere. SSZ-13 with stronger acid can catalyze the hydrogenation of aromatics, which can inhibit the formation of polycyclic aromatic hydrocarbons. This contributes to prolonging the reaction lifetime.

**3.6. Probe Experiment and DFT Calculation.** In the syngas-to-propane reaction over ($CuZnAlO_x$ + ZSM-5)/SSZ-13, DME is first produced in the upper bed. The highly selective propane is primarily related to the conversion mechanism of DME over SSZ-13. Therefore, we systematically compared the reaction behaviors of DME conversion in the lower bed. As shown in Figure 4a, in DME conversion over SSZ-13 under a high-pressure $H_2$ atmosphere, product distribution is highly consistent with the syngas-to-propane process (Figure S5) and the propane selectivity is as high as 77.1%. After SSZ-13 was mixed with $CuZnAlO_x$, the selectivity of propane is only 51.7% with 27.5% ethane and 12.1% butane in hydrocarbons. It is attributed to the strong ability of hydrogenation of the Cu-based catalyst, over which alkenes are converted into alkanes. Furthermore, by adding 10 times of inert gas to the feed gas, $C_2-C_4^=$ even reaches up to 80.5% in


https://doi.org/10.1021/acscatal.1c05132
ACS Catal. 2022, 12, 3985−3994

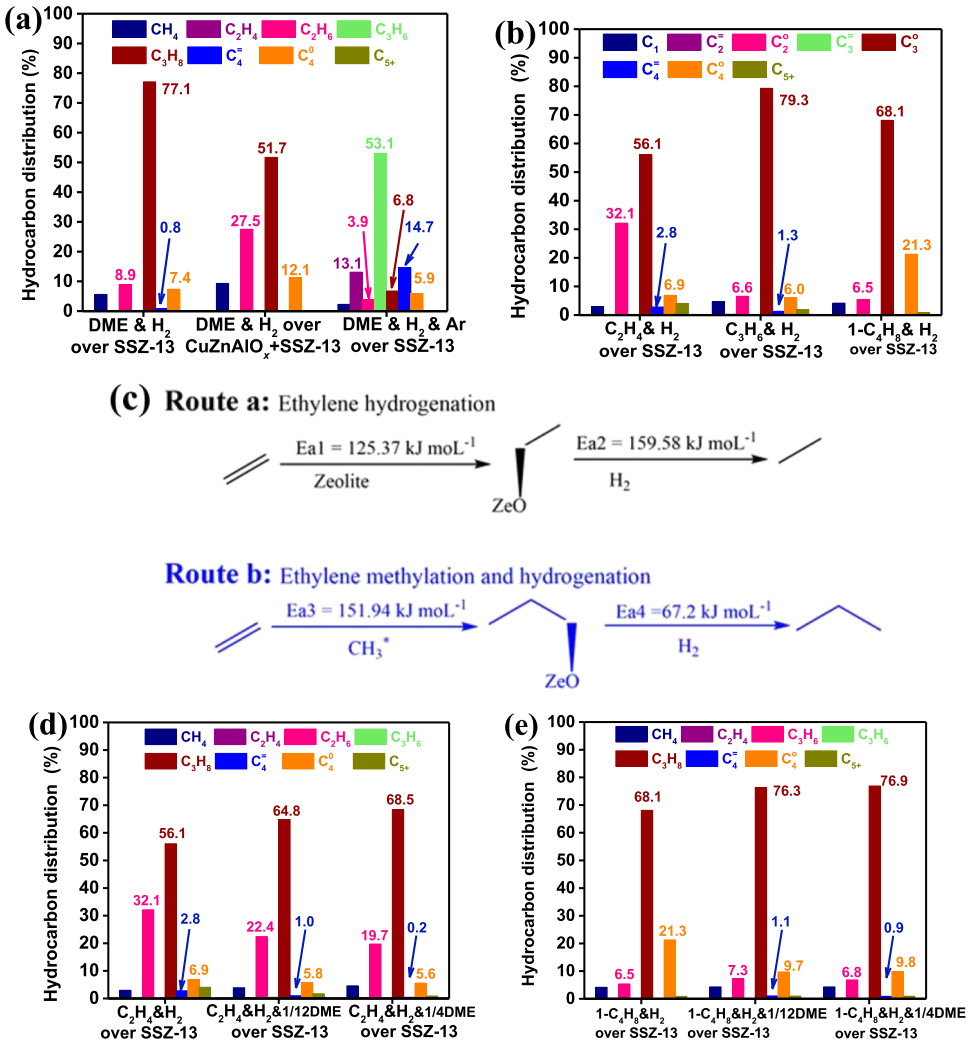


**Figure 4.** (a) DME conversion in high-pressure $H_2$ (or with 10 times of Ar) cofeeding over the SSZ-13 or $CuZnAlO_x$ + SSZ-13 hybrid catalyst; reaction conditions: $T$ = 683 K, $P$ = 5.0 MPa, $H_2$/DME = 17/1, GHSV = 9000 mL $g^{-1}$ $h^{-1}$. (b) $C_2$−$C_4$ olefin conversion in high-pressure $H_2$ over the SSZ-13 zeolite; reaction conditions: $T$ = 683 K, $P$ = 5.0 MPa, $H_2$/olefin =17/1, GHSV = 9000 mL $g^{-1}$ $h^{-1}$; (c) DFT calculation results of ethylene conversion via multiple routes over the SSZ-13 zeolite; (d) ethylene conversion in high-pressure $H_2$ with a small amount of DME over the SSZ-13 zeolite under reaction conditions shown in Table S7; (e) 1-butene conversion in high-pressure $H_2$ with a small amount of DME over the SSZ-13 zeolite under reaction conditions shown in Table S8.

hydrocarbons. These all suggest that $C_2$−$C_4$ olefins could be acted as intermediates to form propane in syngas-to-propane reaction. Combined with GC−MS results shown in Figure 3c, the organic substances in the spent SSZ-13 zeolite are the polymethyl-benzene species, which are generally considered as "hydrocarbon pool" (HCP species) and benefit the formation of olefins.[39,40] Therefore, we confirm that methanol/DME-to-olefins (MTO) reactions must be included in the syngas-to-propane process and $C_2$−$C_4$ olefins are deemed to be the important intermediates to form propane over the SSZ-13 zeolite. Therefore, we investigated the behaviors of $C_2$−$C_4$ olefin conversion catalyzed by SSZ-13 with high-pressure $H_2$ cofeeds. For comparison, the feed rates of the lower olefins based on carbon numbers are equivalent to those of syngas or DME. According to the product distribution (Figure 4b), propane is the dominant product in $C_2$−$C_4^=$ (especially $C_3^=$) conversion with high-pressure $H_2$ cofeeding. Propane selectivity and distribution of other products are all similar to those of the syngas-to-propane process, indicating that highly selective propane is mainly obtained by the hydrogenation of the generated propylene. In addition, propane can also be obtained from ethylene-to-propylene reaction (ETP) or the $C_{4+}$ species hydrocracking to propene process[30,41,42] and then the generated propylene hydrogenation to propane in cascade over the SSZ-13 zeolite. Noticeably, approximately 32% ethane is also produced simultaneously in ethylene conversion under high-pressure $H_2$. Distribution of these products is different from syngas-to-propane in the dual-bed reaction system. This indicates that in the syngas-to-propane reaction network, there may be other reaction paths for the conversion of ethylene to propane besides the ETP process.

In order to get further insights into the reaction network for high propane selectivity, the in situ DRIFTS of DME conversion with $H_2$ over SSZ-13 was explored. A critical intermediate of the methoxy (2930, 2820, and 1052 $cm^{-1}$) species is detected (Figure S6), which is generally involved in the alkene cycle of the MTO process. DFT calculation (results shown in Figure 4c and Table S6) indicates that ethylene could methylate with methoxy species to produce propylene groups (Ea3 = 151.94 kJ·$mol^{-1}$) or be hydrogenated to ethane (Ea2 =


https://doi.org/10.1021/acscatal.1c05132
ACS Catal. 2022, 12, 3985−3994

**Scheme 2. Proposed Reaction Network for Syngas-to-Propane**

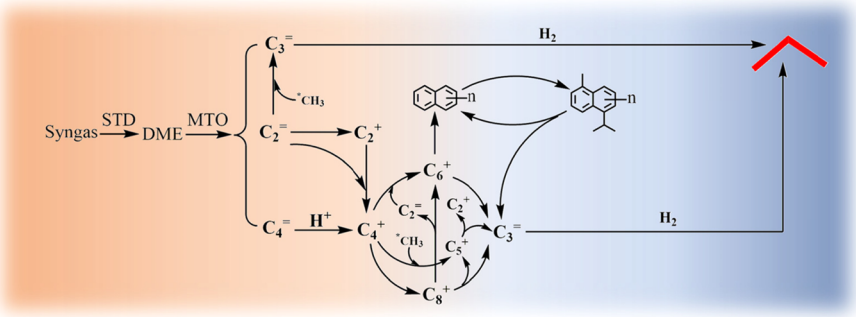


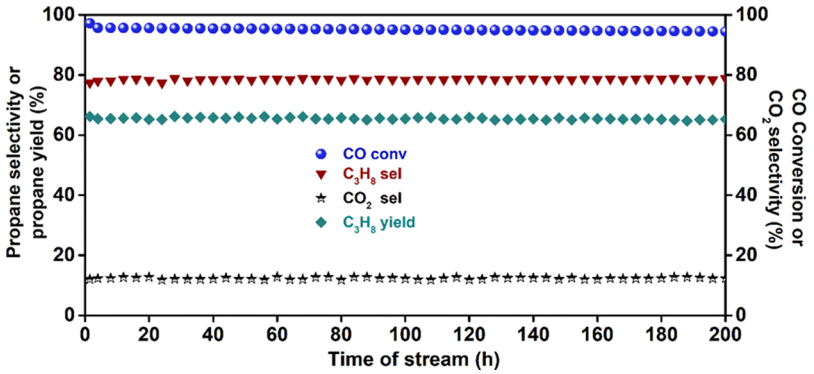


**Figure 5.** Stability of syngas-to-propane reactions over ($CuZnAlO_x$ + ZSM-5)/SSZ-13. $T$ (upper bed) = 533 K, $T$ (lower bed) = 683 K, $P$ = 5.0 MPa, $H_2/CO$ = 7, and GHSV = 4000 mL $g^{-1}$ $h^{-1}$.

159.58 kJ·mol$^{-1}$). The propylene group easily reacts with hydrogen to produce propane (Ea4 = 67.20 kJ·mol$^{-1}$). As a result, over SSZ-13 zeolites, ethylene can be methylated to propylene, which is further hydrogenated to propane. In order to further verify the process that ethylene methylation can produce propane in high-pressure $H_2$, a small amount of DME is added to ethylene conversion reaction under high-pressure $H_2$. Figure 4d and Table S7 indicate that the increase of propane selectivity is equivalent to the decrease of ethane selectivity by introducing a small amount of DME, which proves that the methylation process is more likely to occur in a high-pressure $H_2$ atmosphere than ethylene hydrogenation to ethane. Noticeably, with the introduction of DME, butene selectivity gradually decreases or even disappears, which suggests that butene species may also undergo methylation and then crack to propene, which is further hydrogenated to propane. In order to clarify the contribution of butene in propane generation reaction, apart from butene conversion over SSZ-13 in high-pressure $H_2$, additional experiments of butene conversion with DME over SSZ-13 in high-pressure $H_2$ was also investigated. As shown in Figure 4e and Table S8, with the introduction of DME, propane selectivity in hydrocarbons increases, while butane selectivity decreases, which further proves that butene could also be methylated and then cracked to propene,[30] which is further hydrogenated into propane under high-pressure $H_2$.

**3.7. A Proposed Reaction Network for Syngas-to-Propane.** Based on all above analysis, a proposed reaction network for propane formation with high selectivity is illustrated in Scheme 2. First, DME is produced from syngas over the $CuZnAlO_x$ + ZSM-5 hybrid catalyst in the upper bed. Then, DME is transmitted to SSZ-13 in the lower bed and $C_2$−$C_4$ olefins are generated by the MTO reaction. Ethylene could be continuously converted into propane over SSZ-13 by the following processes: at the beginning, ethylene is protonated by Brønsted acid sites to form a $C_2^+$ carbonium, following a bimolecular dimerization with a second ethylene molecule to form $C_4^+$ carbocations, which readily isomerizes into the other butene isomers. The $C_4^+$ carbocations would polymerize with the third ethylene molecule to form $C_6^+$ intermediates, which can then crack into propylene. Additionally, ethylene also can be directly methylated into propylene. Similarly, the butene-cracking reaction over SSZ-13 catalysts is also a complex process, which involves oligomerization-cracking reactions of $C_6^+$ or $C_8^+$ intermediates to propylene reactions. $C_4^=$ can also be methylated into a $C_5^+$ intermediate, which can further crack into propylene. The cracking of $C_6^+$ and $C_8^+$ intermediates into propylene would be accompanied by cyclization and aromatization processes. According to the previous literature, the naphthalene-based species, such as polymethyl-isopropyl-naphthalenes, play a significant role in generating propylene.[30] Finally, propylene obtained by all above reactions is hydrogenated into propane.

**3.8. Catalytic Performance of Syngas-to-Propane under Optimized Reaction Conditions.** To further investigate the reaction performance, the reaction temperature of the lower bed catalyst, space velocity, and the $H_2/CO$ ratio were tuned to optimize the catalytic performance of syngas-to-propane reaction. Figure S7a shows that propane selectivity increases with the increase of reaction temperature in the lower bed, which is valuable for improving the efficiency of the syngas-to-propane process. Increasing the ratio of $H_2/CO$ in the feedstock can increase the propane selectivity and depress the $CO_2$ selectivity but has little effect on CO conversion


https://doi.org/10.1021/acscatal.1c05132
ACS Catal. 2022, 12, 3985−3994

(Figure S7b). Figure S7c shows that CO conversion and propane selectivity decrease with space velocity rising, but the selectivity of $CO_2$ is slightly changed. Under the optimum reaction conditions of 533 K (upper bed), 683 K (lower bed), 5.0 MPa, $H_2/CO$ = 7/1, and GHSV = 4000 mL $g^{-1}$ $h^{-1}$, ($CuZnAlO_x$ + ZSM-5)/SSZ-13 exhibits an excellent stability within 200 h on stream (Figures 5 and S8). The propane selectivity and CO conversion are kept at approximately 78.6% and 93.6, respectively; meanwhile, the byproduct $CO_2$ selectivity is suppressed as low as 11.8%. Furthermore, the propane yield reaches as high as 65.1% in a single run.

## 4. CONCLUSIONS

In summary, highly selective conversion of syngas-to-propane can be simultaneously achieved over ($CuZnAlO_x$ + ZSM-5)/SSZ-13, a dual-bed reaction system, which consists of an upper bed $CuZnAlO_x$ + ZSM-5 and a lower bed catalyst SSZ-13 ($SiO_2/Al_2O_3$ ratio = 12.5) in the downstream. The propane in the hydrocarbon product can reach 78.6% at CO conversion of 95.7% with less than 15% $CO_2$ selectivity. The propane yield is as high as 65.1%. This dual-bed reaction system exhibits an excellent stability during the 200 h test on stream. For the lower bed SSZ-13 catalyst, strong acid is advantageous to propane formation and beneficial to reducing the coke deposition rate and prolonging lifetime. Probing experiments and DFT calculations imply that highly selective propane formation mainly includes the MTO reaction generating $C_2$−$C_4$ olefins, $C_{4+}$ cracking, and ethylene and butene methylation or oligomerization-cracking processes. Each catalyst of this dual-bed catalyst system can operate under its optimistic conditions. This route would provide a potential method to synthesize one single $C_{2+}$ hydrocarbon from syngas with low $CO_2$ emissions.

## ■ ASSOCIATED CONTENT

### Supporting Information

The Supporting Information is available free of charge at https://pubs.acs.org/doi/10.1021/acscatal.1c05132.

Detailed catalytic results and structural characterization (Figures S1−S8 and Tables S1−S8) (PDF)

## ■ AUTHOR INFORMATION


### Corresponding Authors

**Wenliang Zhu** − *National Engineering Laboratory for Methanol to Olefins and Dalian National Laboratory for Clean Energy, Dalian Institute of Chemical Physics, Chinese Academy of Sciences, Dalian, Liaoning 116023, China*; Email: wlzhu@dicp.ac.cn

**Zhongmin Liu** − *National Engineering Laboratory for Methanol to Olefins and Dalian National Laboratory for Clean Energy, Dalian Institute of Chemical Physics, Chinese Academy of Sciences, Dalian, Liaoning 116023, China; University of Chinese Academy of Sciences, Beijing 100049, China*; orcid.org/0000-0002-7999-2940; Email: liuzm@dicp.ac.cn

### Authors

**Zhaopeng Liu** − *National Engineering Laboratory for Methanol to Olefins and Dalian National Laboratory for Clean Energy, Dalian Institute of Chemical Physics, Chinese Academy of Sciences, Dalian, Liaoning 116023, China; University of Chinese Academy of Sciences, Beijing 100049, China*

**Youming Ni** − *National Engineering Laboratory for Methanol to Olefins and Dalian National Laboratory for Clean Energy, Dalian Institute of Chemical Physics, Chinese Academy of Sciences, Dalian, Liaoning 116023, China*

**Mingbin Gao** − *National Engineering Laboratory for Methanol to Olefins and Dalian National Laboratory for Clean Energy, Dalian Institute of Chemical Physics, Chinese Academy of Sciences, Dalian, Liaoning 116023, China*; orcid.org/0000-0002-7143-2658

**Linying Wang** − *National Engineering Laboratory for Methanol to Olefins and Dalian National Laboratory for Clean Energy, Dalian Institute of Chemical Physics, Chinese Academy of Sciences, Dalian, Liaoning 116023, China*

**Xudong Fang** − *National Engineering Laboratory for Methanol to Olefins and Dalian National Laboratory for Clean Energy, Dalian Institute of Chemical Physics, Chinese Academy of Sciences, Dalian, Liaoning 116023, China; University of Chinese Academy of Sciences, Beijing 100049, China*

**Jie Liu** − *National Engineering Laboratory for Methanol to Olefins and Dalian National Laboratory for Clean Energy, Dalian Institute of Chemical Physics, Chinese Academy of Sciences, Dalian, Liaoning 116023, China; University of Chinese Academy of Sciences, Beijing 100049, China*

**Zhiyang Chen** − *National Engineering Laboratory for Methanol to Olefins and Dalian National Laboratory for Clean Energy, Dalian Institute of Chemical Physics, Chinese Academy of Sciences, Dalian, Liaoning 116023, China*

**Nan Wang** − *National Engineering Laboratory for Methanol to Olefins and Dalian National Laboratory for Clean Energy, Dalian Institute of Chemical Physics, Chinese Academy of Sciences, Dalian, Liaoning 116023, China; University of Chinese Academy of Sciences, Beijing 100049, China*

**Peng Tian** − *National Engineering Laboratory for Methanol to Olefins and Dalian National Laboratory for Clean Energy, Dalian Institute of Chemical Physics, Chinese Academy of Sciences, Dalian, Liaoning 116023, China*

Complete contact information is available at: https://pubs.acs.org/10.1021/acscatal.1c05132


### Notes

The authors declare no competing financial interest.

## ■ ACKNOWLEDGMENTS

We acknowledge the financial support from the National Natural Science Foundation of China (Grant Nos. 21978285, 21991093, and 21991090) and the "Transformational Technologies for Clean Energy and Demonstration," Strategic Priority Research Program of the Chinese Academy of Sciences (Grant No. XDA21030100). We acknowledge Weichen Zhang for his help in the experiment. We acknowledge Mrs. Yanli He and Mr. Yijun Zheng for their help in the characterization of catalysts.

## ■ REFERENCES

(1) Wang, C.; Fang, W.; Wang, L.; Xiao, F.-S. Fischer-Tropsch reaction within zeolite crystals for selective formation of gasoline-ranged hydrocarbons. *J. Energy Chem.* **2021**, *54*, 429−433.

(2) Zhu, C.; Bollas, G. M. Gasoline Selective Fischer-Tropsch Synthesis in Structured Bifunctional Catalysts. *Appl. Catal., B* **2018**, *235*, 92−102.

(3) Kang, J.; Zhang, S.; Zhang, Q.; Wang, Y. Ruthenium Nanoparticles Supported on Carbon Nanotubes as Efficient Catalysts for Selective Conversion of Synthesis Gas to Diesel Fuel. *Angew. Chem., Int. Ed.* **2009**, *48*, 2565−2568.
(4) Cheng, Q.; Tian, Y.; Lyu, S.; Zhao, N.; Ma, K.; Ding, T.; Jiang, Z.; Wang, L.; Zhang, J.; Zheng, L.; Gao, F.; Dong, L.; Tsubaki, N.; Li, X. Confined small-sized cobalt catalysts stimulate carbon-chain growth reversely by modifying ASF law of Fischer−Tropsch synthesis. *Nat. Commun.* **2018**, *9*, 3250−3259.
(5) Torres Galvis, H. M.; Bitter, J. H.; Khare, C. B.; Ruitenbeek, M.; Dugulan, A. i.; De Jong, K. P. Supported Iron Nanoparticles as Catalysts for Sustainable Production of Lower Olefins. *Science* **2012**, *335*, 835−838.
(6) Zhong, L.; Fei, Y.; An, Y.; Zhao, Y.; Sun, Y.; Li, Z.; Lin, T.; Lin, Y.; Qi, X.; Dai, Y.; Gu, L.; Hu, J.; Jin, S.; Shen, Q.; Wang, H. Cobalt carbide nanoprisms for direct production of lower olefins from syngas. *Nature* **2016**, *538*, 84−87.
(7) Jiao, F.; Li, J.; Pan, X.; Xiao, J.; Li, H.; Ma, H.; Wei, M.; Pan, Y.; Zhou, Z.; Li, M.; Miao, S.; Li, J.; Zhu, Y.; Xiao, D.; He, T.; Yang, J.; Qi, F.; Fu, Q.; Bao, X. Selective conversion of syngas to light olefins. *Science* **2016**, *351*, 1065−1068.
(8) Cheng, K.; Gu, B.; Liu, X.; Kang, J.; Zhang, Q.; Wang, Y. Direct and Highly Selective Conversion of Synthesis Gas to Lower Olefins: Design of a Bifunctional Catalyst Combining Methanol Synthesis and Carbon−Carbon Coupling. *Angew. Chem., Int. Ed.* **2016**, *128*, 4803−4806.
(9) Su, J.; Zhou, H.; Liu, S.; Wang, C.; Jiao, W.; Wang, Y.; Liu, C.; Ye, Y.; Zhang, L.; Zhao, Y.; Liu, H.; Wang, D.; Yang, W.; Xie, Z.; He, M. Syngas to light olefins conversion with high olefin/paraffin ratio using $ZnCrO_x$/AlPO-18 bifunctional catalysts. *Nat. Commun.* **2019**, *10*, 1297−1305.
(10) Cheng, K.; Zhou, W.; Kang, J.; He, S.; Wang, Y. Bifunctional Catalysts for One-Step Conversion of Syngas into Aromatics with Excellent Selectivity and Stability. *Chem* **2017**, *3*, 334.
(11) Ramirez, A.; Gong, X.; Caglayan, M.; Nastase, S.-A. F.; Abou-Hamad, E.; Gevers, L.; Cavallo, L.; Chowdhury, A. D.; Gascon, J. Selectivity descriptors for the direct hydrogenation of $CO_2$ to hydrocarbons during zeolite-mediated bifunctional catalysis. *Nat. Commun.* **2021**, *12*, 5914−5926.
(12) Chen, Y.; Gong, K.; Jiao, F.; Pan, X.; Hou, G.; Si, R.; Bao, X. C−C Bond Formation in Syngas Conversion over Zinc Sites Grafted on ZSM-5 Zeolite. *Angew. Chem., Int. Ed.* **2020**, *59*, 6529−6534.
(13) Jiao, F.; Pan, X.; Gong, K.; Chen, Y.; Li, G.; Bao, X. Shape-Selective Zeolites Promote Ethylene Formation from Syngas via a Ketene Intermediate. *Angew. Chem., Int. Ed.* **2018**, *57*, 4692−4696.
(14) Li, G.; Jiao, F.; Miao, D.; Wang, Y.; Pan, X. Selective conversion of syngas to propane over $ZnCrO_x$-SSZ-39 OX-ZEO catalysts. *J. Energy Chem.* **2019**, *36*, 141−147.
(15) Ramirez, A.; Ticali, P.; Salusso, D.; Cordero-Lanzac, T.; Ould-Chikh, S.; Ahoba-Sam, C.; Bugaev, A. L.; Borfecchia, E.; Morandi, S.; Signorile, M.; Bordiga, S.; Gascon, J.; Olsbye, U. Multifunctional Catalyst Combination for the Direct Conversion of $CO_2$ to Propane. *JACS Au* **2021**, *1*, 1719−1732.
(16) Arslan, M. T.; Ali, B.; Gilani, S. Z. A.; Hou, Y.; Wei, F. Selective Conversion of Syngas into Tetramethylbenzene via an Aldol-Aromatic Mechanism. *ACS Catal.* **2020**, *10*, 2477−2488.
(17) Liu, Z.; Ni, Y.; Fang, X.; Zhu, W.; Liu, Z. Highly converting syngas to lower olefins over a dual-bed catalyst. *J. Energy Chem.* **2021**, *58*, 573−576.
(18) Ni, Y.; Wang, K.; Zhu, W.; Liu, Z. Realizing high conversion of syngas to gasoline-range liquid hydrocarbons on a dual-bed-mode catalyst. *Chem. Catal.* **2021**, *1*, 383−392.
(19) Ni, Y.; Liu, Z.; Tian, P.; Chen, Z.; Fu, Y.; Zhu, W.; Liu, Z. A dual-bed catalyst for producing ethylene and propylene from syngas. *J. Energy Chem.* **2021**, *66*, 190−194.
(20) Baltes, C.; Vukojevi, S.; Schüth, F. Correlations between synthesis, precursor, and catalyst structure and activity of a large set of CuO/ZnO/Al2O3 catalysts for methanol synthesis. *J. Catal.* **2008**, *258*, 334−344.
(21) Liu, Z.; Ni, Y.; Hu, Z.; Fu, Y.; Fang, X.; Jiang, Q.; Chen, Z.; Zhu, W.; Liu, Z. Insights into effects of ZrO2 crystal phase on syngas-to-olefin conversion over ZnO/ZrO2 and SAPO-34 composite catalysts. *Chin. J. Catal.* **2022**, *43*, 877−884.
(22) Guisnet, M.; Magnoux, P. Coking and deactivation of zeolites. Influence of the pore structure. *Appl. Catal.* **1989**, *54*, 1−27.
(23) Liu, X.; Zhou, W.; Yang, Y.; Cheng, K.; Kang, J.; Zhang, L.; Zhang, G.; Min, X.; Zhang, Q.; Wang, Y. Design of efficient bifunctional catalysts for direct conversion of syngas into lower olefins via methanol/dimethyl ether intermediates. *Chem. Sci.* **2018**, *9*, 4708−4718.
(24) Fujimoto, K.; Saima, H.; Tominaga, H. O. Synthesis gas conversion utilizing mixed catalyst composed of CO reducing catalyst and solid acid: IV. Selective synthesis of $C_2$, $C_3$, and $C_4$ paraffins from synthesis gas. *J. Catal.* **1985**, *94*, 16−23.
(25) Zhang, Q.; Li, X.; Asami, K.; Asaoka, S.; Fujimoto, K. Synthesis of LPG from synthesis gas. *Fuel Process. Technol.* **2004**, *85*, 1139−1150.
(26) Zhang, Q.; Li, X.; Asami, K.; Asaoka, S.; Fujimoto, K. Direct synthesis of LPG fuel from syngas with the hybrid catalyst based on modified $Pd/SiO_2$ and zeolite. *Catal. Today* **2005**, *104*, 30−36.
(27) Ge, Q.; Li, X.; Kaneko, H.; Fujimoto, K. Direct synthesis of LPG from synthesis gas over Pd−Zn−Cr/Pd-$\beta$ hybrid catalysts. *J. Mol. Catal. A: Chem.* **2007**, *278*, 215−219.
(28) Fujimoto, K.; Saima, H.; Tominaga, H. O. Hydrogenation of carbon monoxide on carbon monoxide reducing catalyst and solid acid. 6. Selective production of $C_3$ and $C_4$ hydrocarbons from synthesis gas. *Ind. Eng. Chem. Res.* **1988**, *27*, 920−926.
(29) Pradhan, S.; Reddy, A. S.; Devi, R. N.; Chilukuri, S. Copper-based catalysts for water gas shift reaction: Influence of support on their catalytic activity. *Catal. Today* **2009**, *141*, 72−76.
(30) Dai, W.; Sun, X.; Tang, B.; Wu, G.; Li, L.; Guan, N.; Hunger, M. Verifying the mechanism of the ethene-to-propene conversion on zeolite H-SSZ-13. *J. Catal.* **2014**, *314*, 10−20.
(31) Dai, W.; Wang, X.; Wu, G.; Guan, N.; Hunger, M.; Li, L. Methanol-to-Olefin Conversion on Silicoaluminophosphate Catalysts: Effect of Brønsted Acid Sites and Framework Structures. *ACS Catal.* **2011**, *1*, 292−299.
(32) Yang, L.; Yan, T.; Wang, C.; Dai, W.; Wu, G.; Hunger, M.; Fan, W.; Xie, Z.; Guan, N.; Li, L. Role of Acetaldehyde in the Roadmap from Initial Carbon−Carbon Bonds to Hydrocarbons during Methanol Conversion. *ACS Catal.* **2019**, *9*, 6491−6501.
(33) Kiricsi, I.; Förster, H.; Tasi, G.; Nagy, J. B. Generation Characterization, and Transformations of Unsaturated Carbenium Ions in Zeolites. *Chem. Rev.* **1999**, *99*, 3367−3370.
(34) Borodina, E.; Kamaluddin, H. S. H.; Meirer, F.; Mokhta, M.; Al-Thabaiti, S. A.; Asiri, A. M.; Basahel, S. N.; Ruiz-Martinez, J.; Weckhuysen, B. M. Influence of the Reaction Temperature on the Nature of the Active and Deactivating Species During Methanol-to-Olefins Conversion over H-SAPO-34. *ACS Catal.* **2017**, *7*, 5268−5281.
(35) Borodina, E.; Meirer, F.; Lezcano-González, I.; Mokhtar, M.; Asiri, A. M.; Al-Thabaiti, S. A.; Basahel, S. N.; Ruiz-Martinez, J.; Weckhuysen, B. M. Influence of the Reaction Temperature on the Nature of the Active and Deactivating Species during Methanol to Olefins Conversion over H-SSZ-13. *ACS Catal.* **2015**, *5*, 992−1003.
(36) Tian, P.; Wei, Y.; Ye, M.; Liu, Z. Methanol to Olefins (MTO): From Fundamentals to Commercialization. *ACS Catal.* **2015**, *5*, 1922−1938.
(37) Zhao, X.; Li, J.; Tian, P.; Wang, L.; Li, X.; Lin, S.; Guo, X.; Liu, Z. Achieving a Superlong Lifetime in the Zeolite-Catalyzed MTO Reaction under High Pressure: Synergistic Effect of Hydrogen and Water. *ACS Catal.* **2019**, *9*, 3017−3025.
(38) Arora, S. S.; Nieskens, D. L. S.; Malek, A.; Aditya, B. Lifetime improvement in methanol-to-olefins catalysis over chabazite materials by high-pressure $H_2$ co-feeds. *Nat. Catal.* **2018**, *1*, 666−672.
(39) Ni, Y.; Liu, Y.; Chen, Z.; Yang, M.; Liu, H.; He, Y.; Fu, Y.; Zhu, W.; Liu, Z. Realizing and Recognizing Syngas-to-Olefins Reaction via a Dual-Bed Catalyst. *ACS Catal.* **2019**, *9*, 1026−1032.


https://doi.org/10.1021/acscatal.1c05132
*ACS Catal.* 2022, 12, 3985−3994

(40) Lin, S.; Zhi, Y.; Chen, W.; Li, H.; Lou, C.; Wu, X.; Zeng, S.; Xiao, J.; Zheng, A.; Wei, Y.; Liu, Z. Molecular Routes of Dynamic Autocatalysis for Methanol-to-Hydrocarbons Reaction. *J. Am. Chem. Soc.* **2021**, *143*, 12038−12052.
(41) Dahl, I. M.; Kolboe, S. On the Reaction Mechanism for Hydrocarbon Formation from Methanol over SAPO-34: 2. Isotopic Labeling Studies of the Co-reaction of Propene and Methanol. *J. Catal.* **1996**, *161*, 304−309.
(42) Dahl, I. M.; Kolboe, S. On the Reaction Mechanism for Hydrocarbon Formation from Methanol over SAPO-34: I. Isotopic Labeling Studies of the Co-Reaction of Ethene and Methanol. *J. Catal.* **1994**, *149*, 458−464.





https://doi.org/10.1021/acscatal.1c05132
*ACS Catal.* 2022, 12, 3985−3994